Cascade mixing in $Al_xGa_{1-x}As/GaAs$ during sputter profiling by noble-gas ions

M. K. Linnarsson* and B. G. Svensson
Royal Institute of Technology, Solid State Electronics, P.O. Box E229, SE-164 40 Kista-Stockhom, Sweden
(Received 6 May 1999)

The effect of cascade mixing on profile broadening during secondary-ion mass spectrometry (SIMS) analysis has been thoroughly investigated for $Al_xGa_{1-x}As/GaAs$ structures of five different compositions ($x=0.1$, 0.3, 0.5, 0.73, or 1) and layers with varying thicknesses (from one monolayer to 1000 Å). The SIMS analyses were performed using primary sputtering ions of $^{20}Ne^+$, $^{40}Ar^+$, $^{84}Kr^+$, and $^{136}Xe^+$ with an impact energy (E) ranging from 1.8 to 13.2 keV and an angle of incidence, with respect to the surface normal (θ), from 62° to 35°. Within the experimental accuracy, the decay length of the trailing edge was found to be proportional to $E^{1/2}\cos\theta$ where the proportionality constant displays a relatively weak dependence on primary ion mass. However, the leading edge is strongly affected by the extension of the collision cascade as demonstrated by a comparison of the results for the different ions at a given energy. As long as the cascade is fully developed before reaching an interface no dependence on the sample depth is obtained for the profile broadening. Furthermore, the decay length for the trailing edges is extracted in the dilute limit and no effect of the marker thickness or the x value is revealed. A numerical treatment of the profile broadening within a diffusional model, where the diffusion coefficient is assumed to be proportional to the energy deposited in elastic collisions, gives a surprisingly good agreement with the experimental data. [S0163-1829(99)08543-4]

I. INTRODUCTION

An issue of major concern for sputter profiling of semiconductor structures concerns the fundamental processes determining the depth resolution. This is, indeed, of the utmost relevance since today superlattices and quantum-well structures with atomically sharp interfaces and dopant distributions can be fabricated. Over the last decades substantial efforts have been made to improve our understanding of the effects of ion bombardment of such structures and some mechanisms have been identified, e.g., cascade mixing,[1–3] primary recoil mixing,[4] surface roughening,[5–7] radiation-enhanced diffusion[8–12] and segregation,[9–11] so-called Gibbsian surface segregation,[9,12–15] and preferential sputtering.[16–18] Normally, these mechanisms are active simultaneously but a carefully designed experiment may ideally isolate the effects of one particular mechanism of interest.

In this study we focus on the transport of target atoms by recoil mixing which can be divided into two contributions: primary and cascade mixing. The first one emerges from direct collisions between the incident ions and target atoms; a small number of relatively energetic recoiling atoms will be preferentially generated in the direction of the incident ions and will contribute to a shift and broadening of a given initial profile. However, the influence of primary mixing is generally of minor importance. Cascade mixing is in most cases the major effect, and Guinan and Kinney[19] described the evolution of a cascade by three stages, first an initial displacement/collision phase, second a relaxation phase where a large fraction of generated defects recombine spontaneously, and finally, a third phase where the lattice is ''cooled down'' to the ambient temperature applying the concept of thermal spike.[2] Both the initial and the third phase involves a relocation of target atoms but the nature of the atomic transport is different. The collisional phase is ballistic and perhaps the best understood part in the mixing process; a binary description of the collisional events is found to apply as long as the density of elastic energy deposition is small. Analytical models based on Boltzmann's linear transport equation as well as Monte Carlo simulations show good agreement with experimental data for sputtering yields and ion penetration depths,[4,20–22] and the ballistic collisions occur typically on a time scale[23] of 10^{-13}–10^{-12} s. It should also be mentioned that during the collisional phase interstitials and vacancies are created which survive during longer times and may facilitate diffusion in later stages.

If the density of energy deposited in elastic collisions becomes high enough ($\geqslant$1–10 eV/atom) the binary collision approximation starts to break down and many-body collision must be taken into account. The energy of the impinging ions is divided between a large number of low-energy recoiling target atoms involved in the collision cascade and the energy distribution becomes of Maxwell-Boltzmann type. The concept of a local temperature and thermal spike[24] can be introduced and the excess energy associated with the collision cascade is distributed in the target according the classical laws of heat conduction. For ion energies typical of sputter depth profiling (1–10 keV) $\sim 10^3$–10^4 target atoms are set in motion by each impinging ion, and the cascade quenches in $\sim 10^{-11}$ s after reaching equilibrium with the surrounding lattice.

It is interesting to note that the diffusion transport equation and the linear Boltzmann transport equation are complementary forms of the continuity equation, and an attractive approach for the modeling of collision-induced transport of target atoms is to adopt the well-known formalism established within the theory for diffusion.[25–28] Several experimental results reveal substantially larger mixing of target atoms than predicted by models taking only the collisional contribution into account,[29] and this supports the idea that the mass transport occurs predominantly during the cooling

 ©1999 The American Physical Society

stage of a cascade. Assuming that the mixing contribution from binary collisions is negligible, several authors[30–33] have developed a phenomenological model which exhibits good agreement with experimental data for mixing of metallic bilayers by ions with energies in excess of ~100 keV. The model is also found to be valid at the ion energies employed for sputter depth profiling,[34] and the similarity between mixing at high and low ion energies ($\geqslant$100 and $\leqslant$10 keV) can be attributed to the fractal nature of the collision cascade.[33]

On the basis of a model by Ma[35] for mixing in the dilute limit of thin markers in a metal matrix, Zalm and Vriezema[36] derived a simple expression for a characteristic scaling factor (decay length), with the dimension of length, describing the profile broadening during sputtering by low-energy ions. A major modification in Ref. 36 compared to the model by Ma[35] concerns the effect of the eroding surface and only those ions are considered where the surface has come into the vicinity of the marker. The decay length λ is predicted to be proportional to the square root of the incident ion energy (E) multiplied by the cosine of the angle of incidence (θ) (with respect to the surface normal) where the proportionality constant is independent of the projectile mass. This is in direct contrast to relations proposed by other authors assuming that λ scales with the ion penetration depth.[37–39] However, the type of relation suggested by Zalm and Vriezema has been supported by several recent experiments,[40–42] although the predicted independence of the projectile mass has not been addressed in detail. A similar scaling of the profile broadening with $E^{1/2}\cos\theta$, but including a dependence on the primary ion mass, has been derived by Andersen[22] using a different starting point where the cascade mixing is treated in a diffusional manner based on collision theory.

In this work a systematic secondary-ion mass spectrometry (SIMS) study of cascade mixing in superlattice structures of $Al_xGa_{1-x}As/GaAs$ has been performed using noble-gas ions for sputtering. The effects on profile broadening by ion mass, impact ion energy, angle of incidence, quantum-well thickness, x value (Al content), and sample depth have been investigated. The variations in erosion rate and ionization yield with x are also examined. In particular, the influence of projectile mass on cascade mixing is studied in detail and a close proportionality between the decay length of the trailing edge and $E^{1/2}\cos\theta$ is obtained. The proportionality constant displays only a weak dependence on ion mass while the opposite holds for the leading edge. In the latter case the extension of the collision cascade is found to play a crucial role and the experimental data are compared with simulations using a diffusional model where the diffusivity is assumed to be proportional to the elastic energy deposition.

II. EXPERIMENTAL DETAILS

$Al_xGa_{1-x}As/GaAs$ ($x=0.1$, 0.3, 0.5, 0.73, or 1) superlattice structures with different layer thickness were prepared by metal-organic vapor phase epitaxy (MOVPE) and by molecular-beam epitaxy (MBE). In Figs. 1(a)–1(c) schematic diagrams of the sample structures are shown. The thickness of the individual layers and the Al concentration were determined by high-resolution x-ray diffraction using a four-crystal monochromator, except for the samples with $x=0.1$ where the GaAs and $Al_{0.1}Ga_{0.9}As$ peaks could not be clearly resolved. This holds also for the sample with a periodicity of two monolayers where the signal intensity from the first pair of satellites was below the background level. In order to facilitate the x-ray measurements an additional package of 20 identical $Al_xGa_{1-x}As/GaAs$ periods were included, as indicated by Figs. 1(a) and 1(c). Homogeneous layers of $Al_xGa_{1-x}As$ ($x=0.1$, 0.3, 0.5, 0.73, or 1) with a thickness of ~2 μm were used for studying the x dependence of the $^{27}Al^+$ secondary-ion intensity and the erosion rate. A cap surface layer of GaAs was grown on the AlAs samples to prevent oxidation of Al. Furthermore, a photoluminescence study of the interface quality indicates an abruptness of the interfaces of less than 3 ML.

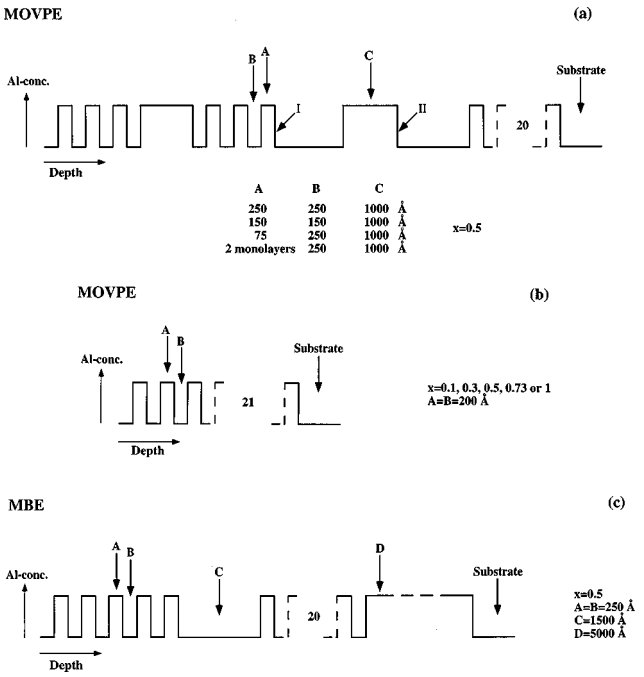

FIG. 1. Schematic diagrams of the sample structures used for analysis; (a) and (b) are grown by MOVPE and (c) by MBE.

The SIMS analyses were performed in a Cameca ims $4f$ instrument. Primary sputtering ions of $^{20}Ne^+$, $^{40}Ar^+$, $^{84}Kr^+$, and $^{136}Xe^+$ were employed with an impact energy ranging from 1.8 to 13.2 keV where the sample voltage (4.5 kV) and the plasma energy in the ion source (0.2 keV) are taken into account. The primary ion energy and the angle of incidence, θ cannot be varied independently in the ims $4f$ configuration and an increase of the energy from 1.8 to 13.2 keV results in a decrease of θ from 62° to 35° with respect to the surface normal. When estimating θ, correction has been made for the change in angle with respect to the optical axis caused by the deflection plates for beam positioning.[43] The primary ion beam was rastered over an area of $250\times250\ \mu m^2$ and secondary ions of $^{27}Al^+$ were collected from the central part of this area (analyzing diameter ~8 μm). The dynamical range was more than three decades for all the x values. During profiling the stability of the primary ion current was better than ±3% and the erosion rate was in the range 0.5–3 Å/s. Series of measurements of the crater depth as a function of sputter time have been used to extract the erosion rates. Crater depths were determined by an Alphastep-200 surface stylus profilometer. The pressure in the sample chamber was $<4\times10^{-9}$ Torr during analysis.

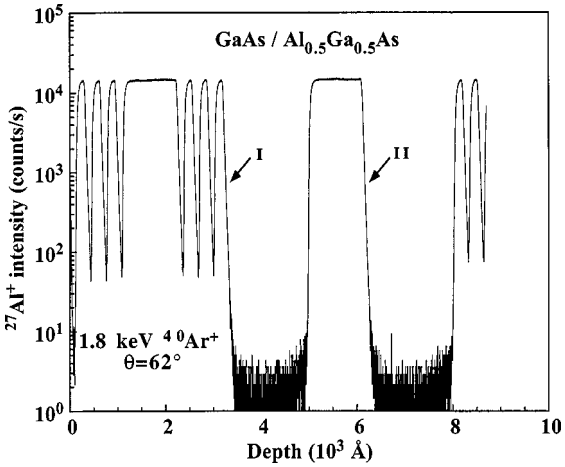

FIG. 2. SIMS measurements of the Al concentration versus depth obtained from a $Al_{0.5}Ga_{0.5}As/GaAs$ structure using $^{40}Ar^+$ ions at an impact energy of 1.8 keV ($\theta=62°$). Decay lengths are extracted from the trailing edges marked with I and II.

III. RESULTS

A typical depth profile of Al obtained from a $Al_{0.5}Ga_{0.5}As/GaAs$ structure during sputtering by $^{40}Ar^+$ ions using an impact energy of 1.8 keV ($\theta=62°$) is shown in Fig. 2. The original scale for the sputtering time is converted into depth using not only the total crater depth but also taking into account the dependence of the erosion rate on the Al content. In Fig. 3(a) the relative erosion rate is depicted as a function of x for six different impact energies of $^{40}Ar^+$ ions ranging from 1.8 to 8.2 keV, and the values are normalized with respect to the rate in GaAs. As E increases the decrease in the erosion rate with x becomes stronger and at 8.2 keV there is a difference of almost a factor of 2 between AlAs and GaAs. For each energy, a linear approximation is made in Fig. 3(a) and an analogous treatment is also made for $^{20}Ne^+$, $^{84}Kr^+$, and $^{136}Xe^+$ ions; these relations are then employed in the conversion of sputtering time to depth for the measured profiles. Moreover, the so-obtained depth scale is compared with x-ray data and the two sets of values for the period of the structures agree within 3%. Figure 3(b) displays the ratio between the secondary-ion intensity of $^{27}Al^+$ and the erosion rate as a function of x, and irrespective of ion energy the increase in the ionization with x show a pronounced diviation from a linear relation.

From the measured profiles, exemplified by Fig. 2, the exponential decay length λ_{meas} of the trailing edges of the Al profiles has been evaluated according to the relation

$$\lambda_{meas}=\frac{z_1-z_2}{\ln\frac{I_{z_2}}{I_{z_1}}}, \tag{1}$$

where I is the secondary-ion intensity of $^{27}Al^+$, z_1 and z_2 are the depths corresponding to I_{z_1} and I_{z_2}, respectively. A least-squares fit of the experimental data by an exponential relation was typically performed between 10% and 0.1% of the maximum intensity. Within the experimental accuracy the values of λ_{meas} obtained from MOVPE and MBE grown samples are identical, as illustrated in Fig. 4 for

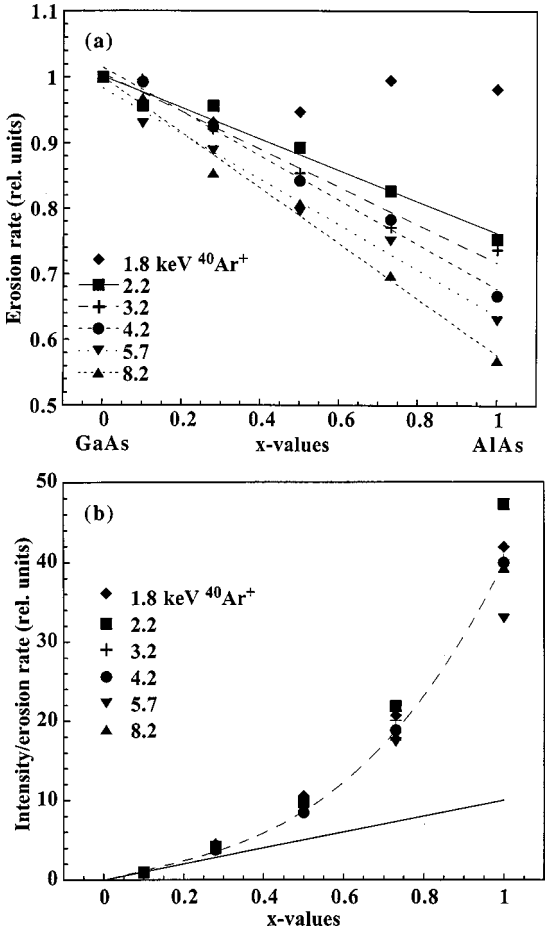

FIG. 3. Erosion rate (a) and ratio between secondary-ion intensity and erosion rate (b) as a function of Al concentration (x values) for $^{40}Ar^+$ ions at impact energies of 1.8, 2.2, 3.2, 4.2, 5.7, and 8.2 keV.

$Al_{0.5}Ga_{0.5}As/GaAs$ structures profiled by $^{40}Ar^+$ sputtering ions. In the intensity interval used for extraction of λ_{meas} the addition of ion-induced and intrinsic slopes can be written as

$$\lambda^n_{ion}=\lambda^n_{meas}-\lambda^n_{intr} \tag{2}$$

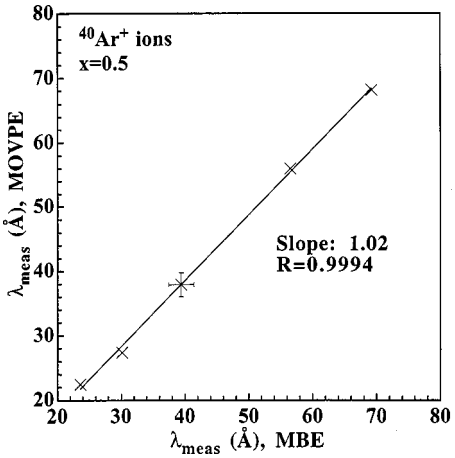

FIG. 4. Comparison between measured decay lengths (λ_{meas}) obtained from MOVPE and MBE grown samples with $x=0.5$ using $^{40}Ar^+$ ions. Error bars indicate a relative accuracy of ±5%.

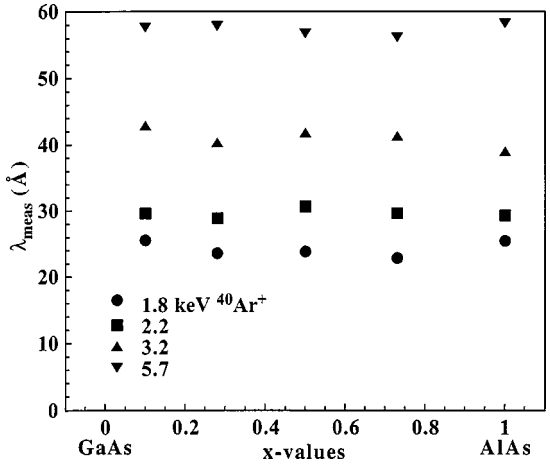

FIG. 5. Decay length (λ_{meas}) versus Al concentration (x values) for the sample structure described in 1(b) obtained with 1.8, 2.2, 3.2, and 5.7 keV $^{40}Ar^+$ ions.

with $n \approx 4$.[44,45] For the structures used in this study, $\lambda_{intr} \approx 2$ Å, which corresponds to an interfacial abruptness of ~ 3 ML, and the approximation $\lambda_{ion} \approx \lambda_{meas}$ is valid within a high degree of accuracy.

In Fig. 5 λ_{meas} is depicted versus x for four different energies of $^{40}Ar^+$ ions during analysis of the sample structure described in Fig. 1(b). No dependence on x is revealed and this holds for all the noble-gas ions used. Moreover, except for the most oblique angle of incidence (lowest energy) where tilted crater bottoms cause a degradation in the depth resolution, no dependence of the extracted λ_{meas} values on sample depth and layer thickness is observed. This is shown in Figs. 6 and 7 for $x = 0.5$ and $^{40}Ar^+$ ions, and similar results hold for all the combinations of ions, energies, and sample structures employed in this study.

The average value of λ_{meas} extracted at interfaces I and II [Fig. 1(a)] is displayed in Fig. 8(a) as a function of $E^{1/2}\cos\theta$ for $^{40}Ar^+$ ions, and a linear relation is found to hold with a high correlation coefficient. Fig. 8(b) shows the results for all

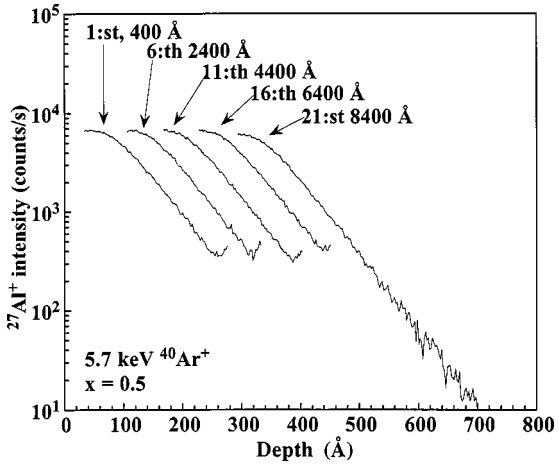

FIG. 6. $^{27}Al^+$ signal as a function of depth for the trailing edges at the interfaces 1, 6, 11, 16, and 21 in the sample structure given in 1(b) and with $x = 0.5$. Analysis was performed with $^{40}Ar^+$ ions at an impact energy of 5.7 keV. The depth scales for the interfaces 6, 11, 16, and 21 have been displaced in order to facilitate a comparison with interface 1.

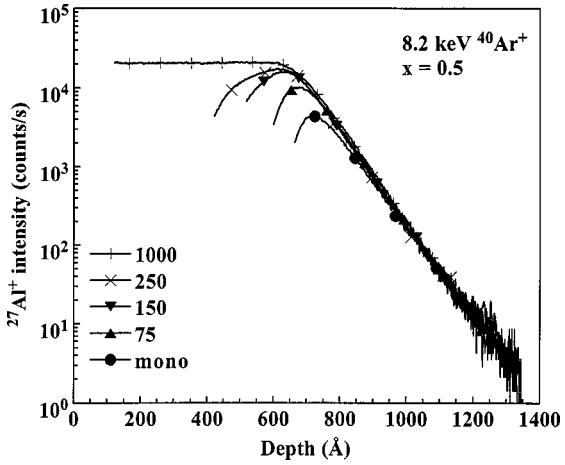

FIG. 7. $^{27}Al^+$ signal as a function of depth for the trailing edges after passing $Al_{0.5}Ga_{0.5}As$ layers of various thicknesses (mono, 75, 150, 250, and 1000 Å) using the sample structure in 1(a). Analysis was performed with $^{40}Ar^+$ ions at an impact energy of 8.2 keV. The depth scales have been displaced in order to facilitate a comparison.

the noble-gas ions used, and a small but significant decrease of the linear slope with increasing ion mass is revealed. The absolute values of the slope are depicted versus the ion mass

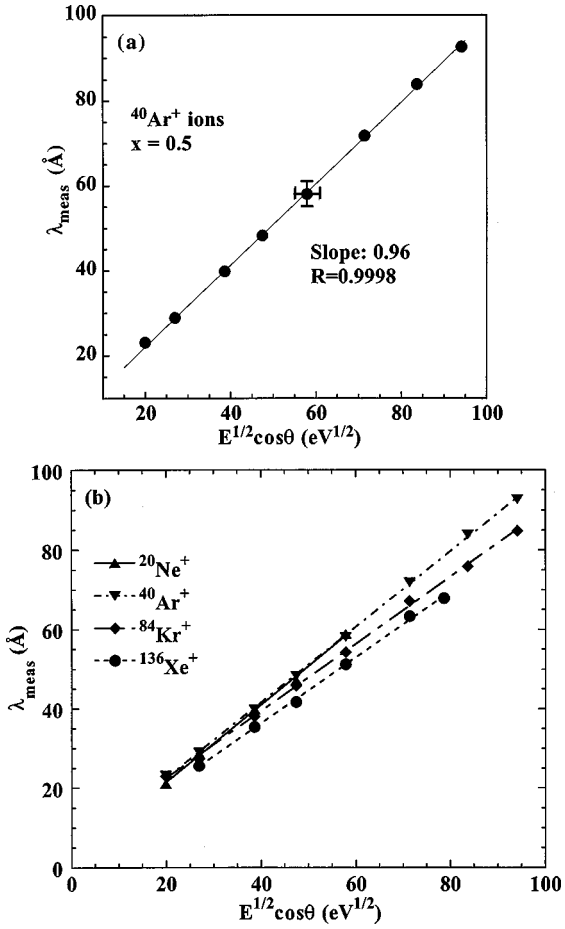

FIG. 8. Decay length (λ_{meas}) of the trailing edge at the interfaces I and II in 1(a) versus $E^{1/2}\cos\theta$ for (a) $^{40}Ar^+$ and (b) $^{20}Ne^+$, $^{40}Ar^+$, $^{84}Kr^+$, and $^{136}Xe^+$ sputtering ions. Error bars indicate a relative accuracy of $\pm 5\%$.

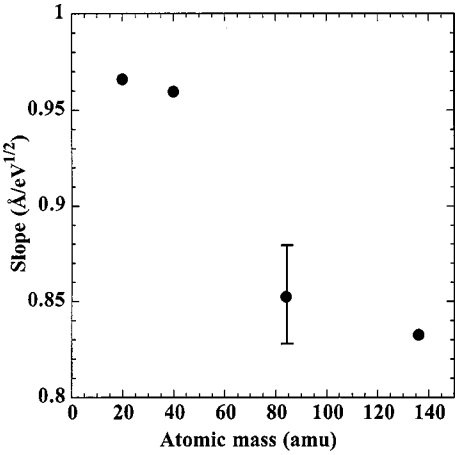

FIG. 9. Absolute values of the slopes between λ_{meas} and $E^{1/2}\cos\theta$, extracted from the data in 8(b), versus ion mass. Error bars indicate a relative accuracy of ±3%.

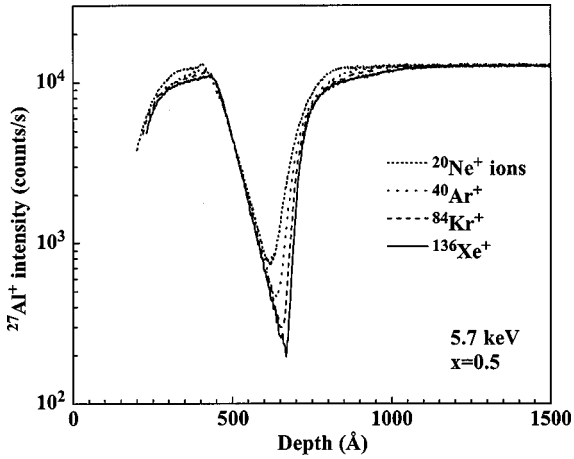

FIG. 11. $^{27}Al^+$ signal in a small depth interval of the sample structures in 1(a), using $^{20}Ne^+$, $^{40}Ar^+$, $^{84}Kr^+$, and $^{136}Xe^+$ sputtering ions at an impact energy of 5.7 keV.

in Fig. 9 and a relative difference of ~15% is found between $^{20}Ne^+$ and $^{136}Xe^+$ ions.

In contrast to that for the trailing edge, the leading edge is not truly exponential but more Gaussian in shape, which is illustrated in Fig. 10 showing the $^{27}Al^+$ signal from three $GaAs/Al_{0.5}Ga_{0.5}As$ interfaces located at different depths. A broadening with increasing depth is observed and this effect is also found to exhibit a pronounced mass dependence, Fig. 11. The dynamic range of the $^{27}Al^+$ signal decreases by almost a factor of 4 for $^{20}Ne^+$ relative to that for $^{136}Xe^+$, and applying an exponential approximation $\lambda_{\text{leading edge}}(^{20}Ne^+) \approx 2\lambda_{\text{leading edge}}(^{136}Xe^+)$ at 5.7 keV.

IV. DISCUSSION

A. Some basic considerations

The relative influence of direct projectile (Ne, Ar, Kr, Xe) -target collision (recoil implantation) and target-target atom collision (cascade mixing) on profile broadening can be estimated through Monte Carlo simulations using the transport

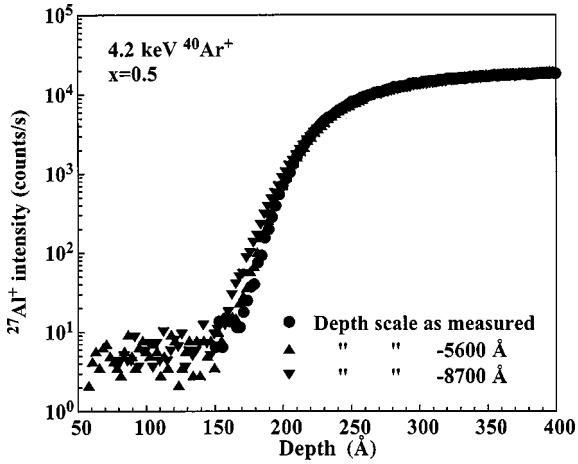

FIG. 10. $^{27}Al^+$ signal as a function of depth for the leading edge at three $GaAs/Al_{0.5}Ga_{0.5}As$ interfaces located at different depths [sample structure given in 1(a)]. 4.2 keV $^{40}Ar^+$ ions were used for profiling. The depth scale for the two deep interfaces have been displaced in order to facilitate a comparison.

of ions in matter code (TRIM, version −90).[46] The relocation caused by direct projectile-target collision contributes with a minor part to the total number of displacements varying roughly from 10% for the highest energies used in this study to ~30% for 1.8 keV $^{20}Ne^+$ ions. The first collisions in a cascade are anisotropic and can produce both a shift and a broadening of a given initial profile; a few target atoms will receive large momenta in the forward direction, which also have been reported as tails in high-energy ion beam mixing studies,[47,48] but these direct knock-on recoils are rare events. The low-energy fraction of the cascade may, however, be regarded as isotropic mainly causing broadening of the original profiles. The initial energy distribution of recoiling atoms in a cascade is strongly weighted towards low energies and a major part is close to the displacement energy threshold (E_d). Assuming that nuclear stopping dominates, Sigmund[49] has shown that the recoil density, scales as $1/T^2$ where T is the energy of the recoiling atoms. This scaling predicts that in the energy range studied less than 3% of the recoiling atoms will receive energies above 500 eV. Furthermore, the projected range in GaAs for 500 eV ions ranging from $^{136}Xe^+$ to $^{20}Ne^+$ varies only between 16–19 Å indicating that most atomic motion will be short and on the order of a few atomic distances. This short range of penetration for the major part of displaced atoms in combination with that target-target atom collisions dominate suggest that the total amount of deposited energy determines the degree of mixing rather than the projected range of the primary ions. On the other hand, the projected range of the primary ions reflects where the energy is deposited. The contribution of electronic energy losses to the total stopping is typically less than 10% in the energy range studied. For simplicity, this small contribution from the electronic stopping is neglected in the following discussion and the power-law approximation, with an exponent $m \approx 0.19-0.25$, is found to apply for the elastic collisions, according to the so-called universal stopping power in the energy range of interest.[50,51]

B. Extension of the collision cascade

A marker profile starts to be affected by the sputtering ions first when the collision cascade reaches the profile and

will undergo continuous redistribution until it is fully sputtered away. If a marker is situated at a depth larger than the extension of the cascade a dynamical equilibrium is reached and no degradation with depth should be obtained, as shown in Fig. 6 for five identical structures located at different depths.

The amount of broadening of a profile is related to the distance of relocation of the recoiling atoms and the total number of displacements before the marker is sputtered away. An important property is the relation between the sputtering yield and the total amount of displacements in a cascade where the intersection of the cascade with the target surface determines the sputtering yield. The main part of the sputtered ions originates from the top surface layer but there is also some contribution from several atomic layers below the surface. The mixing starts when the collision cascade reaches the interface of the marker layer and this being so the leading edge cannot be broader than the extension of the cascade. As seen in Fig. 11, $^{20}Ne^+$ has the broadest leading edge followed by $^{40}Ar^+$, $^{84}Kr^+$, and $^{136}Xe^+$ in correspondence to the relative extension of the respective cascades. A rough estimation gives an extension of $\geqslant$125 Å for the cascade induced by 5.7 keV $^{20}Ne^+$ ions and gradually smaller values for the heavier ions. These estimates are supported by simulations discussed in Sec. IV C.

The leading edge is much steeper than the trailing edge where the marker atoms are distributed in the mixing volume and will be pushed deeper into the sample. Since the slope is higher for the leading edge the effect of surface roughening and interface abruptness is more pronounced than for the trailing edge, and in Fig. 10, a small broadening of the leading edge of the two deeper positioned interfaces is seen relative to that of the shallow interface. This is attributed to the development of a small surface roughness and/or a small tilt of the crater bottom. The thickness of the GaAs top layer is 250 Å, which should be enough to establish steady-state conditions and a full development of the collision cascade, (4.2 keV $^{40}Ar^+$) even at the most shallow interface.

C. Relation between profile broadening and primary ion parameters

High vacancy production (or elastic energy deposition) per impact ion will increase both the sputtering yield and the cascade mixing since the two processes have the same origin. The degree of cascade mixing is, however, expected to have an upper limit where the material is fully homogenized. Andersen[22] has treated the cascade mixing as a random-walk problem and looked at the average number of displacements (N) before sputtering, $N=n(E)/Y$, where Y is the sputtering yield and $n(E)$ the number of displacements within a cascade. The total amount of displacements is proportional to the energy E of the impinging ions assuming linear cascades where the displacement energy threshold is small relative to E and cascade multiplication applies; $n(E)=bE$, where b is a constant primarily depending on the target material and to some extent on the ion. Furthermore, Sigmund[52] has derived the following dependence of the sputtering yield Y on the angle of incidence (θ),

$$Y(\theta)=Y(0°)\cos\theta^{-f} \tag{3}$$

where $f\approx 5/3$ for not too glancing incidence ($\theta\leqslant 70°$) and with $m\approx 1/3$ for mass ratio between target atoms and ions less than 3.

Neglecting the influence of the moving surface and assuming stationary boundary conditions a diffusional process will broaden an original δ function to a Gaussian distribution with a variance $\sigma=(4Dt)^{1/2}$, where D is the diffusion coefficient chosen as a constant and t is the diffusion time. According to the Einstein relation[53] the diffusion constant (for amorphous material) can be expressed as

$$D=\Gamma R^2/6, \tag{4}$$

where Γ is a jumping frequency given by $\Gamma=N/t$ in our case. R is a step length chosen as a constant value (being of the order of a few atomic distances). Most recoils in the cascade have penetration lengths $\leqslant$20 Å and therefore, the assumption of a constant R independent of E appears reasonable. As a result the broadening can now be written as,

$$\sigma=2R(b/6)^{1/2}Y(0°)^{-1/2}E^{1/2}\cos^{5/6}\theta, \tag{5}$$

where $b/Y(0°)$ shows only a small variation for the different types of ions and energies used in this study. This being so gives $\sigma\sim E^{1/2}\cos^{5/6}\theta$ a result close to that observed experimentally for λ in Figs. 8(a) and 8(b), and the observed weak mass dependence may be attributed to the factor $b/Y(0°)$. Here, it should be pointed out that a general least-squares fit of $\lambda_{meas}/\cos\theta$ as a function of E gives an exponent of 0.54, in accordance with the linear relation in Fig. 8. Further, using inert ions different groups have reported a close proportionality between λ and $E^{1/2}\cos\theta$ where the proportionality constant is found to be essentially independent of the ion mass,[40–42,54,55] consistent with Eq. (5) and the data in Fig. 9.

Andersen's model[22] gives a rather general outline of the effect of cascade mixing. The treatment of mixing phenomena within the diffusion concept has been further developed by several authors[26–28,56] where both moving boundary conditions and a variation of D with depth have been included. For a numerical treatment of profile broadening including these effects we have used a diffusional model suggested by Tuck and co-workers[57] as the starting point. This approach can be considered as a simplified version of the IMPEUS model,[56] valid in the dilute limit and with a minimum number of fitting parameters. In Ref. 57 it was assumed that the number of atomic jumps between adjacent planes, under a short time (dt), scales with the number of atoms available to jump at the beginning of the time interval dt. This number will vary somewhat during the time interval, but the variations are, normally not too large and as a first approximation, a constant value can be assumed. Another approximation concerns the change in atomic density if more atoms leave a plane than those entering and at some stage a relaxation of the material will take place. This has, however, been ignored in the calculations which are expected to be most valid in a dilute concentration regime. In all simulations, a distance of 2 Å is used for adjacent planes, a value considered only as a numerical parameter but of the same order of magnitude as the nearest-neighbor distance in GaAs (2.45 Å). Further, the sputtering is treated as an instantaneous step change by one atomic layer each time and the jumping frequency varies with depth in proportion to the energy transferred to the recoils, as obtained from TRIM calculations. The only fitting

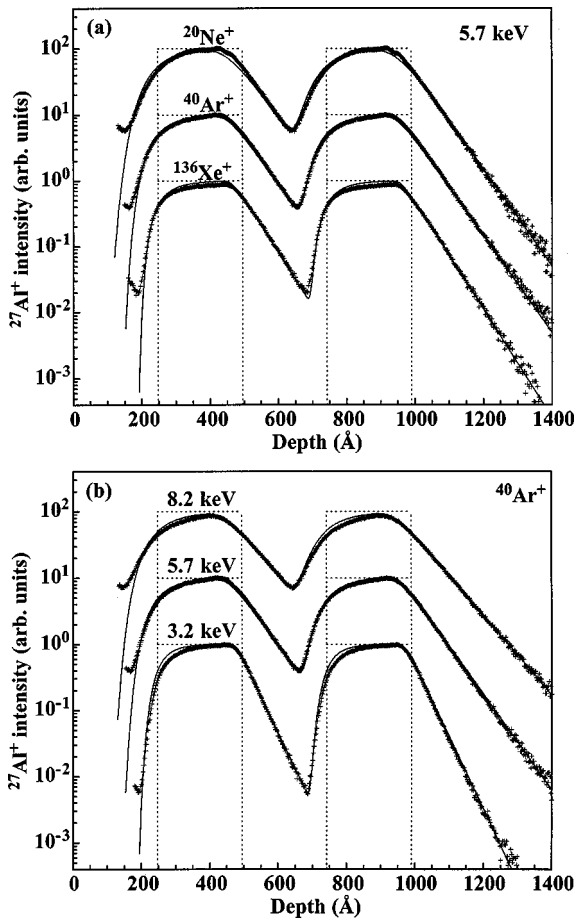

FIG. 12. Comparison between measurements (data points) and simulations (full line) for a selected region of the sample structure in 1(a) ($x=0.5$). (a) sputtering by $^{20}Ne^+$, $^{40}Ar^+$, and $^{136}Xe^+$ ions at an impact energy of 5.7 keV and (b) sputtering by $^{40}Ar^+$ ions at impact energies of 3.2, 5.7, and 8.2 keV. The original sample structure is included as a dotted line.

parameter used is the time of duration of the cascade before another layer is removed, and in Figs. 12(a) and 12(b), measured and simulated profiles are compared for $^{20}Ne^+$, $^{40}Ar^+$, and $^{136}Xe^+$ sputter ions. The agreement is surprisingly good both as a function of ion energy and ion mass and even at higher concentrations where some of the approximations made in the calculations are questionable. Moreover, an extraction of the relative sputtering yields (assuming a constant b) at 5.7 keV from the simulated curves gives a value for $^{136}Xe^+$ twice that for $^{40}Ar^+$. The same relation is obtained within a few percent from a comparison of the measured erosion rate per impact ion for $^{136}Xe^+$ and $^{40}Ar^+$ at 5.7 keV, while such a comparison between $^{20}Ne^+$ and $^{40}Ar^+$ gives a difference of less than 20%. A similar comparison for different Ar energies, [Fig. 12(b)], gives a nice agreement between 8.2 and 5.7 keV (better than 8%) but a slightly larger difference is obtained between 3.2 and 5.7 keV (60%). These results support the validity of treating b as a constant, independent of the ion masses and ion energies employed in this study.

A linear dependence of λ on $E^{1/2}\cos\theta$ has also been derived by Zalm and Vriezema[36] but using a totally different concept based on thermal spikes. The collision phase is neglected and the mixing is assumed to take place only in the

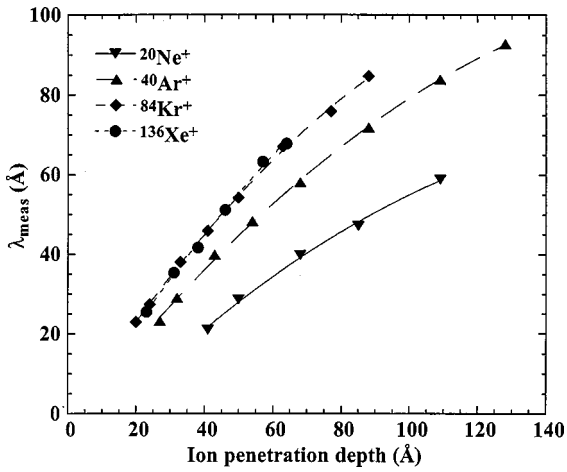

FIG. 13. Measured decay length (λ_{meas}) as a function of penetration depth for $^{20}Ne^+$, $^{40}Ar^+$, $^{84}Kr^+$, and $^{136}Xe^+$ sputtering ions. The penetration depth is estimated by calculations using the TRIM code.

subsequent relaxation phase. Zalm and Vriezema[36] started with a semiempirical expression suggested by the Caltech group[33] for the broadening in metallic bilayers by high-energy ions ($\geqslant$100 keV). The validity of some of the approximations made in Ref. 36 is limited but anyhow they arrived at a proportionality between λ and $E^{1/2}\cos\theta$ where the proportionality constant is also independent of the ion mass.

Some authors[37–39] have tried to scale broadening with the penetration depth (at normal incidence; the penetration depth equals the projected range, R_p). For low ion energies where the power cross approximation is valid, R_p scales with E^{2m} and a choice of $m=0.25$ (a rather realistic value as estimated from the universal screening function[51]) gives $R_p \sim E^{1/2}$. To estimate the penetration depth from R_p, the angular dependence is normally taken into account through a $\cos\theta$ relation, and again, we end up with $\lambda \sim R_p\cos\theta \sim E^{1/2}\cos\theta$. However, the use of R_p rather than $E^{1/2}$ introduces a pronounced ion mass dependence which is not supported by the experimental data λ_{meas}, as shown in Fig. 13. The penetration depths employed in Fig. 13 are estimated from TRIM calculations (taken into account the angle of incidence) and their absolute values are anticipated to be correct within 15–20%

Finally, it should be pointed out that the erosion rate is lower for AlAs than for GaAs [Fig. 3(a)]. Assuming that the escape depth of sputtered atoms is roughly the same for the two compounds the main part of the variation in erosion rate with x can be attributed to (i) a difference in surface binding energy and (ii) a change in ''surface volume'' relative to the whole cascade volume. The latter contribution seems reasonable since for a lighter matrix the cascade is more extended and the relative ''surface portion'' of the cascade becomes smaller with less energy deposited in the near surface region. This also implies more atomic displacements prior to sputtering of AlAs and consequently a higher degree of mixing provided that complete saturation is not established. Taking into account (i) and (ii) an estimation of the ratio between the erosion rates for GaAs and AlAs gives 1.6 for 8.2 keV Ar^+ ions where the energy deposition in the nuclear collisions is

obtained from TRIM. This is in reasonable agreement with the results in Fig. 3(a) where the variation in erosion rate is a factor of ~1.8 between AlAs and GaAs for 8.2 keV Ar^+ ions. On the basis of these results, it is not obvious that the λ_{meas} values should be independent of x, as shown Fig. 5, or unaffected by the thickness of the marker layer, Fig. 7. However, the λ_{meas} values are evaluated in a dilute concentration limit where the matrix can be regarded as GaAs and the cascade becomes ''fully'' developed in a ''GaAs-like environment'' before reaching the position where the λ_{meas} values are determined.

V. SUMMARY

A systematic study of profile broadening caused by cascade mixing during SIMS analysis of $Al_xGa_{1-x}As$/GaAs structures, with atomically sharp interfaces, has been undertaken using noble-gas ions for sputtering. The decay length λ_{meas} of the (declining) trailing edges for ^{27}Al is found to be proportional to $E^{1/2}\cos\theta$ with a relative variation of the proportionality constant of less than 15% for ions ranging from $^{20}Ne^+$ to $^{136}Xe^+$. The decay lengths are extracted in the dilute limit where the x value and the thickness of the marker layer are immaterial. Further, when steady-state conditions are established and the collision cascade is fully developed, no depth dependence of λ_{meas} is revealed. A relation of this type between λ_{meas} and E and θ is fully consistent with the diffusion theory for collisional mixing, which even accounts for the small influence by ion mass if the jumping frequency is assumed to be proportional to the elastic energy deposition.

In direct contrast to that for the trailing edge, the leading edge exhibits a pronounced dependence on the primary ion mass, where sputtering by $^{20}Ne^+$ ions, being the lightest ion used and having the most extended collision cascade, shows the broadest leading edge. Excellent agreement is demonstrated between the measured data for the full profile (including leading and trailing edges as well as the peak region) and simulations using a diffusional treatment of the profile broadening where the diffusion constant varies with depth and is proportional to the elastic energy deposition. It is evident from the simulations that the broadening of the leading edge is close to the extension of the collision cascade and that substantial mixing takes place within the cascade. Moreover, both the experiments and the simulations give a sputtering yield that decreases with decreasing ion mass, as expected because of a higher elastic energy deposition close to the surface for the heavy ions; e.g., at 5.7 keV the sputtering yield is a factor of ~2 higher for $^{136}Xe^+$ compared to $^{40}Ar^+$ ions.

ACKNOWLEDGMENTS

Financial support was partly received from the Swedish Board of Technical Development and the Swedish Natural Science Research Council.

*Author to whom correspondence should be addressed. FAX: +46 8 752 77 82. Electronic address: marga@ele.kth.se

[1] R. S. Averback, Nucl. Instrum. Methods Phys. Res. B **15**, 675 (1986).
[2] D. A. Thompson, Radiat. Eff. **56**, 105 (1981).
[3] S. Hofmann, J. Vac. Sci. Technol. B **10**, 316 (1992).
[4] U. Littmark and W. O. Hofer, Nucl. Instrum. Methods **168**, 329 (1980).
[5] G. Carter, Vacuum **47**, 409 (1996).
[6] O. Auciello, Radiat. Eff. **60**, 1 (1982).
[7] R. M. Bradley and J. M. E. Harper, J. Vac. Sci. Technol. A **6**, 2390 (1988).
[8] R. Sizmann, J. Nucl. Mater. **69&70**, 386 (1968).
[9] N. Q. Lam and H. Wiedersich, Nucl. Instrum. Methods Phys. Res. B **18**, 471 (1987).
[10] L. E. Rehn, R. S. Averback, and P. R. Okamoto, Mater. Sci. Eng. **1985**, 1 (1985).
[11] L. E. Rehn and N. Q. Lam, L. Mater. Eng. **9**, 205 (1987).
[12] N. Q. Lam, Surf. Interface Anal. **12**, 65 (1988).
[13] R. Kelly, Nucl. Instrum. Methods Phys. Res. B **18**, 388 (1987).
[14] J. Kirschner, Nucl. Instrum. Methods Phys. Res. B **7/8**, 742 (1985).
[15] S. Hofmann, Scanning **III**, 1071 (1985).
[16] R. Shimizu, Nucl. Instrum. Methods Phys. Res. B **18**, 486 (1987).
[17] P. Sigmund and A. Oliva, Nucl. Instrum. Methods Phys. Res. B **82**, 269 (1993).
[18] R. Kelly, Surf. Interface Anal. **7**, 1 (1985).
[19] M. W. Guinan and J. H. Kinney, J. Nucl. Mater. **103&104**, 1319 (1981).
[20] H. M. Urbassek and U. Conrad, Nucl. Instrum. Methods Phys. Res. B **69**, 413 (1992).
[21] W. Eckstein and J. P. Biersack, Appl. Phys. A: Solids Surf. **37**, 95 (1985).
[22] H. H. Andersen, Appl. Phys. **18**, 131 (1979).
[23] M. T. Robinson, Phys. Rev. B **40**, 10 717 (1989).
[24] G. H. Vineyard, Radiat. Eff. **29**, 245 (1976).
[25] S. Matteson, Appl. Phys. Lett. **39**, 288 (1981).
[26] R. Collins and G. Carter, Radiat. Eff. **54**, 235 (1981).
[27] G. Carter, R. Collins, and D. A. Thompson, Radiat. Eff. **55**, 99 (1981).
[28] B. V. King and I. S. T. Tsong, J. Vac. Sci. Technol. A **2**, 1443 (1984).
[29] B. M. Pain and R. S. Averback, Nucl. Instrum. Methods Phys. Res. B **7/8**, 666 (1985).
[30] W. L. Johnson, Y.-T. Cheng, and M. Van Rossum *et al.*, Nucl. Instrum. Methods Phys. Res. B **7/8**, 657 (1985).
[31] M. Van Rossum, Y.-T. Cheng, and M.-A. Nicolet *et al.*, Appl. Phys. Lett. **46**, 610 (1985).
[32] Y.-T. Cheng, T. W. Workman, and M.-A. Nicolet *et al.*, in *Studies of a Phenomenological Model of Ion Mixing*, edited by M. O. Thompson, S. T. Picraux, and J. S. Williams, MRS Symposia Proceedings No. 74 (Materials Research Society, Pittsburgh, 1987), p. 419.
[33] Y.-T. Cheng, Mater. Sci. Rep. **5**, 45 (1990).
[34] Y.-T. Cheng, E.-H. Cirlin, and B. M. Clemens *et al.*, in *A Comparison Between High- and Low-Energy Ion Mixing*, edited by L. E. Rehn, J. E. Greene, and F. A. Smidt, MRS Symposia Proceedings No. 128 (Materials Research Society, Pittsburgh, 1989), p. 419.
[35] E. Ma, Nucl. Instrum. Methods Phys. Res. B **58**, 194 (1991).
[36] P. C. Zalm and C. J. Vriezema, Nucl. Instrum. Methods Phys. Res. B **67**, 495 (1992).
[37] W. Vandervorst and F. R. Sheperd, J. Vac. Sci. Technol. A **5**, 313 (1987).

[38] J. C. Dupuy, G. Prudon, and C. Dubois *et al.*, Nucl. Instrum. Methods Phys. Res. B **85**, 379 (1994).
[39] M. Meuris, W. Vandervorst, and J. Jackman, J. Vac. Sci. Technol. A **9**, 1482 (1991).
[40] M. K. Linnarsson, B. G. Svensson, and Z. F. Paska *et al.*, Nucl. Instrum. Methods Phys. Res. B **85**, 395 (1994).
[41] M. Petravic, B. G. Svensson, and J. S. Williams, Appl. Phys. Lett. **62**, 278 (1993).
[42] M. Meuris, W. Vandervorst, and P. De Bisschop *et al.*, Appl. Phys. Lett. **54**, 1531 (1989).
[43] M. Meuris, P. De Bisschop, and J. F. Leclair *et al.*, Surf. Interface Anal. **14**, 739 (1989).
[44] P. C. Zalm and R. C. M. de Kruif, Appl. Surf. Sci. **70/71**, 73 (1993).
[45] J. Cardenas and B. G. Svensson, in *Secondary Ion Mass Spectrometry, SIMSXI*, edited by G. Gillen, R. Lareau, J. Bennett, and F. Stevie (Wiley, Chichester, 1998), p. 335.
[46] J. P. Biersack and L. G. Haggmark, Nucl. Instrum. Methods **174**, 257 (1980).
[47] T. C. Banwell and M.-A. Nicolet, edited by G. K. Hubler, O. W. Holland, C. R. Clayton, and C. W. White, *Depth Dependence and Chemical Effects in Ion Mixing of Ni on SiO2*, MRS Symposia Proceedings No. 27 (Materials Research Society, Pittsburgh, 1984), p. 109.
[48] L. A. Christel and J. F. Gibbons, Nucl. Instrum. Methods **182/183**, 187 (1981).
[49] P. Sigmund, Rev. Roum. Phys. **17**, 823 (1972); **17**, 969 (1972); **17**, 1079 (1972).
[50] J. Lindhard, M. Scharff, and H. E. Schiøtt, Mat. Fys. Medd. K. Dan. Vidensk. Selsk. **33**, 14 (1963).
[51] J. F. Ziegler, J. P. Biersack, and U. Littmark, *The Stopping and Range of Ions in Solids* (Pergamon, New York, 1985).
[52] P. Sigmund, Phys. Rev. **184**, 383 (1969).
[53] P. Shewmon, *Diffusion in Solids*, 2nd ed. (Minerals, Metals & Materials Society, Warrendale, 1989).
[54] M. K. Linnarsson, B. G. Svensson, and T. G. Andersson *et al.*, Appl. Surf. Sci. **70/71**, 40 (1993).
[55] K. Wittmaack and D. B. Poker, Nucl. Instrum. Methods Phys. Res. B **47**, 224 (1990).
[56] R. Badheka, M. Wadsworth, and D. G. Armour *et al.*, Surf. Interface Anal. **15**, 550 (1990).
[57] B. Tuck, *Atomic Diffusion in III-V Semiconductors* (IOP, Bristol, 1988).